Communication

Modulation Doping of GaAs/AlGaAs Core–Shell Nanowires With Effective Defect Passivation and High Electron Mobility

Jessica L Boland, Sonia Conesa-Boj, Patrick Parkinson, Gözde Tütüncüoglu, Federico Matteini, Daniel Rüffer, Alberto Casadei, Francesca Amaduzzi, Fauzia Jabeen, Christopher L Davies, Hannah J Joyce, Laura M. Herz, Anna Fontcuberta i Morral, and Michael B Johnston

Nano Lett., **Just Accepted Manuscript** • DOI: 10.1021/nl504566t • Publication Date (Web): 20 Jan 2015

Modulation Doping of GaAs/AlGaAs Core–Shell Nanowires With Effective Defect Passivation and High Electron Mobility

Jessica L. Boland,[†] Sonia Conesa-Boj,[‡] Patrick Parkinson,[†] Gözde Tütüncüoglu,[‡] Federico Matteini,[‡] Daniel Rüffer,[‡] Alberto Casadei,[‡] Francesca Amaduzzi,[‡] Fauzia Jabeen,[‡] Christopher L. Davies,[†] Hannah. J. Joyce,[¶] Laura M. Herz,[†] Anna Fontcuberta i Morral,[‡] and Michael B. Johnston[*,†]

Department of Physics, University of Oxford, Clarendon Laboratory, Parks Road, Oxford, OX1 3PU, United Kingdom, Laboratory of Semiconductor Materials, École Polytechnique Fédérale de Lausanne (EPFL), CH-1015 Lausanne, Switzerland, and University of Cambridge, Centre for Advanced Photonics and Electronics, 9 JJ Thomson Avenue, Cambridge CB3 0FA, United Kingdom

E-mail: m.johnston@physics.ox.ac.uk

[*]To whom correspondence should be addressed
[†]Department of Physics, University of Oxford
[‡]Laboratory of Semiconductor Materials, École Polytechnique Fédérale de Lausanne (EPFL)
[¶]University of Cambridge, Centre for Advanced Photonics and Electronics

Abstract

Reliable doping is required to realise many devices based on semiconductor nanowires. Group III–V nanowires show great promise as elements of high–speed optoelectronic devices, but for such applications it is important the electron mobility is not compromised by the inclusion of dopants. Here we show that GaAs nanowires can be n-type doped with negligible loss of electron mobility. Molecular beam epitaxy was used to fabricate modulation doped GaAs nanowires with $Al_{0.33}Ga_{0.67}As$ shells that contained a doped layer of Si dopants. We identify the presence of the doped layer from a high–angle annular dark field scanning electron microscopy cross-section image. The doping density, carrier mobility and charge carrier lifetimes of these n-type nanowires and nominally undoped reference samples were determined using the non–contact method of optical pump terahertz probe spectroscopy. An n-type extrinsic carrier concentration of $1.10 \pm 0.06 \times 10^{16}\,\mathrm{cm}^{-3}$ was extracted, demonstrating the effectiveness of modulation doping in GaAs nanowires. The room temperature electron mobility was also found to be high at $2200 \pm 300\,\mathrm{cm}^2\mathrm{V}^{-1}\mathrm{s}^{-1}$ and importantly minimal degradation was observed compared with undoped reference nanowires at similar electron densities. In addition, modulation doping significantly enhanced the room temperature photoconductivity and photoluminescence lifetimes to $3.9 \pm 0.3\,\mathrm{ns}$ and $2.4 \pm 0.1\,\mathrm{ns}$ respectively, revealing that modulation doping can passivate interfacial trap states.

Keywords

GaAs, modulation doping, delta doping, terahertz spectroscopy, photoconductivity, surface plasmon, mobility, photoluminescence

Semiconductor nanowires are attractive in the field of nanotechnology owing to their potential as building blocks for compact ultrafast electronic and optoelectronic devices.[1] They

have already been shown to have a variety of practical applications, from photovoltaics[2–4] to nanoscale lasers[5,6] and light emitting diodes.[7,8] In order to create functional electronic devices, it is necessary to be able to control the charge carrier concentration in these nanowires. One way of implementing this is through deliberate incorporation of dopants to control the nanowire conductivity.

Doping in semiconductor nanowires was first investigated by the Hiruma group, with the demonstration of GaAs p-n junctions.[9] Since then, both bulk n-type and p-type doping have been fabricated in GaAs nanowires.[10–14] Bulk doping has been shown to yield a high doping concentration but at the expense of a reduction in electron mobility resulting from impurity scattering.[15,16] Thus, other doping mechanisms that allow for both a high extrinsic carrier concentration and carrier mobility are of great interest. Modulation doping is one such mechanism, as it has been shown to avoid a decrease in electron mobility at low temperatures for planar semiconductor heterostructures,[17] as ionised impurities are separated from free charge carriers. By applying modulation doping to semiconductor nanowires, it is predicted that their carrier mobility and transport properties could be improved.[18] Thus, the growth and characterisation of such nanostructures has become an important area of research.[19]

In practice, doping of III-V nanowires has been shown to be more difficult than doping of conventional layered devices, with modulation doping, in particular, being a challenging area of research. Dopant incorporation can differ for lateral and axial growth, leading to inhomogeneous doping, compensation or ineffective doping.[20–23] However, in the past few years, advances in the growth of modulation doped nanowires have been made.[18,24–26] Several types of III-V semiconductor heterostructures have been realised, which provide real potential for obtaining high carrier mobilities. For example, a thin InAs nanowire was fabricated that was capped with a 6 nm thick InP shell containing a delta-doping layer at a 3 nm distance from the nanowire core. Even though InAs and InP are lattice mismatched, the structure did not contain any dislocations. The shell provided electrons at the InAs interface and, at the same time, it separated them from the nanowire surface, which also contained

charged species. Electrical transport measurements demonstrated an increase of mobility from $2\,000\,\mathrm{cm^2V^{-1}s^{-1}}$ up to $15\,600\,\mathrm{cm^2V^{-1}s^{-1}}$ at 100 K for this nanostructure.[27]

Since then, other groups have attempted modulation-doped nanowire-based structures for the GaAs/AlGaAs system.[24–26] The optical and electronic properties of GaAs nanowires have been extensively studied[28–32] and growth optimised to give the best electronic performance, making them prime candidates for modulation doping. GaAs/AlGaAs systems also allow the positioning of the delta doping layer to be further away from the conducting channel, which should further increase the carrier mobility. Recently, magneto-conductance measurements on single GaAs nanowires with a modulation-doped structure were published.[26,33] Universal conductance fluctuations indicated a phase coherence length of up to 250 nm in the core of the structure, which should increase as the mobility is improved. For such nanowires, it is important that carrier concentrations and mobilities are accurately evaluated so that the structure can be tailored for optimised electronic performance. This proves difficult using conventional Hall techniques, owing to the quasi-one-dimensional geometry of nanowires and difficulties in fabricating the lateral contacts needed for such measurements.[34] Thus, other non–contact methods, such as Raman spectroscopy, are currently being investigated for accurate analysis of the carrier density in nanowires,[35] yet the evaluation of carrier concentrations and mobilities remains technically difficult.

In this work, we examine the ultrafast carrier dynamics of n-type modulation doped GaAs/AlGaAs core–shell nanowires and assess the effects of doping on electron mobility and carrier lifetime. Measurement of room-temperature photoconductivity was carried out with sub-picosecond resolution via optical pump terahertz–probe (OPTP) spectroscopy.[28] This technique is contact–free and allows the doping density of the nanowires to be extracted accurately at room temperature without artefacts associated with making electrical contacts.[36] To our knowledge, the OPTP technique has not yet been used to determine the carrier concentration in modulation doped nanowires. From OPTP measurements, we show that n-type modulation doping is indeed effective in the core-shell GaAs/AlGaAs nanowires, with an n-

type carrier concentration of $10^{16}\,\mathrm{cm}^{-3}$ measured in the core. More significantly, we show that the high electron mobility is retained through modulation doping and determinate a photoconductivity lifetime of over 3 ns and a photoluminescence lifetime of over 2 ns. Such a long carrier lifetime and maintained high electron mobility at room temperature suggest that modulation doped GaAs could make excellent candidates for optoelectronic devices and that OPTP spectroscopy offers a reliable technique for doping characterisation.

Core–shell GaAs/$Al_{0.33}Ga_{0.67}As$ nanowires were grown on a p-type (111)Si substrate via molecular beam epitaxy (MBE) under conditions which maximise the yield of vertical nanowires (details of the growth parameters are provided in the Supporting Information). The structure of the nanowire heterostructures used in this study is illustrated in Figure 1a, which shows a cross–section of a nanowire perpendicular to its long axis. Rods of GaAs with a diameter of ∼50 nm were coated with 40 nm wide shells of larger bandgap $Al_{0.33}Ga_{0.67}As$. Si impurities were used to produce a dopant layer at a distance of 12 nm from the GaAs/$Al_{0.33}Ga_{0.67}As$ interface with a nominal doping density of $4.5 \pm 0.5 \times 10^{18}\,\mathrm{cm}^{-3}$. Finally, to limit oxidation of the nanowires in air, a thin (5 nm thick) GaAs capping layer was coated on top of the $Al_{0.33}Ga_{0.67}As$ shells. Modulation n-type doping of the GaAs core region of the nanowire is then achieved as a result of donated electrons from the ionised Si donor atoms in the doped region of the large bandgap $Al_{0.33}Ga_{0.67}As$ shell migrating to the lower potential energy of the the GaAs core region. A self-consistent solution of the Schrödinger and Poisson equations for this structure,[37] as shown in Figure 1b and c, illustrates this process. For use as a reference sample, undoped core–shell GaAs/$Al_{0.33}Ga_{0.67}As$ nanowires were also grown via MBE under similar growth conditions. These undoped nanowires had the same geometry and morphology as the modulation doped nanowires, but did not contain the doped layers of Si impurities. Both the modulation doped and undoped nanowires were transferred to z-cut quartz substrates for measurement. A comparison of these two samples then allowed the effects of modulation doping to be examined.

Figure 1a shows a High Angle Annular Dark Field Scanning Transmission Electron Mi-

croscopy (HAADF–STEM) cross–section image of a representative nanowire for the modulation doped sample. A schematic illustration of the core–shell structure has been superimposed on the left side of the STEM image. In this contrast image the brightness is proportional to the atomic number squared, so the darker regions highlight the presence of lighter elements. Thus, the modulation doping can be clearly identified where the doping layer crosses the Al-rich stripes, as marked by the arrows in Figure 1a. Structural characterization in the axial direction confirm that both samples have a similar crystalline structure, namely the zinc–blende crystalline phase with the presence of twin defects (shown in the high resolution TEM images provided in the Supporting Information). Figure 1b shows results from the numerical simulation[37] of the electron density profile for this modulation doped structure. The electron density profile takes into account the doping expected for a 5 nm-thick doping layer and has the same geometry as measured from the TEM images. Figure 1c depicts this electron density profile superposed onto a simulated energy band diagram for the modulation doped sample. It can clearly be seen that the dopant layer is situated in the $Al_{0.33}Ga_{0.67}As$ shell and alters the conduction band profile.

The photoconductivity dynamics of the nanowires were measured at room temperature by the OPTP setup described in the Supporting Information. The nanowires were photoexcited with a near-infrared laser of wavelength 800 nm ($E_{\mathrm{photon}} = 1.55\,\mathrm{eV}$) and pulse duration of 35 fs at fluences between $0.46\,\mu\mathrm{J\,cm^{-2}}$ and $225\,\mu\mathrm{J\,cm^{-2}}$. This wavelength is ideal as electron-hole pairs were only generated in the central core region and capping layer of the nanowire and not in the $Al_{0.33}Ga_{0.67}As$ shell. The photoexcitation induces a change, ΔE, in the transmission of the electric field of terahertz probe pulse, E. The value of $\Delta E/E$ is proportional to the photoinduced conductivity of the nanowires and thereby the change in free carrier concentration[38] (see Supporting Information). The photoinduced conductivity is assumed to arise solely from the photoexcited electrons, as the effective mass of holes is significantly greater than the effective mass of electrons in GaAs.

Figure 2a shows the decay of the free electron concentration with time after photoexcita-

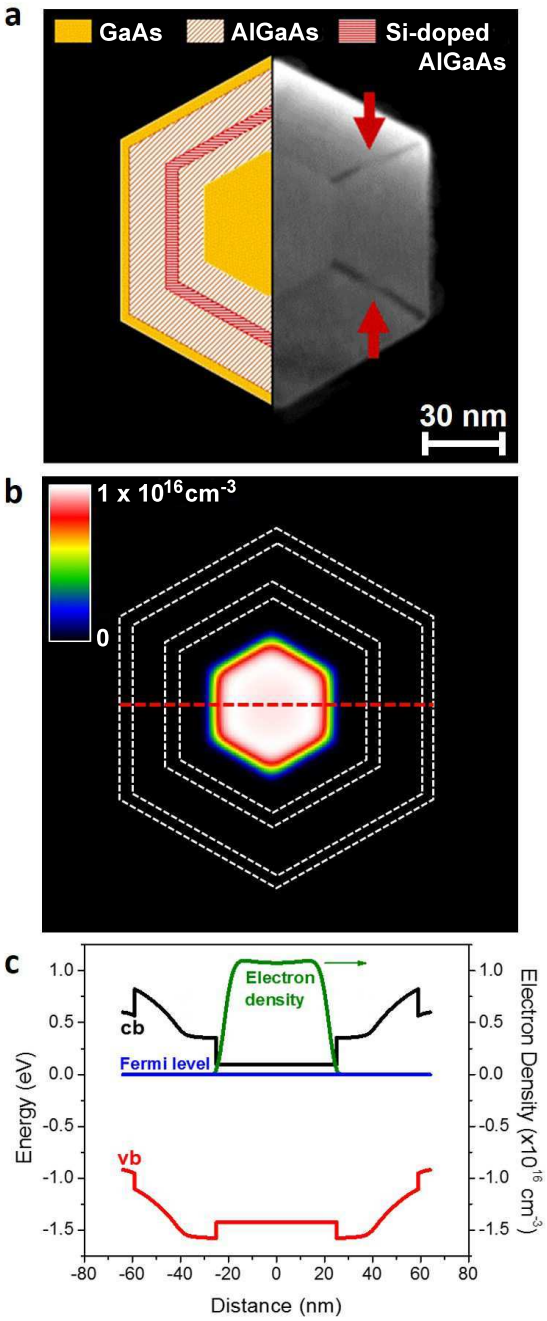

Figure 1: HAADF-STEM cross–section image of a) a representative GaAs/$Al_{0.33}Ga_{0.67}As$ core–shell nanowire with modulation doping. A schematic description of the core–shell structure has been superposed to the left of the STEM image. The arrows indicate the regions with different contrast that correspond to the doped layer crossing the Al-rich segments. b) Nextnano[37] simulation of the electron density profile assuming a nominal doping density of $4.5 \pm 0.5 \times 10^{18}\,\mathrm{cm}^{-3}$ for the modulation-doped nanowire. c) Energy band diagram for modulation-doped nanowire with electron density profile (green line) superimposed. The conduction (valence) band edge is shown in black (red) and the chemical potential or "Fermi level" is represented as the blue line. The red dashed line in b) marks the path to which the band diagram corresponds.

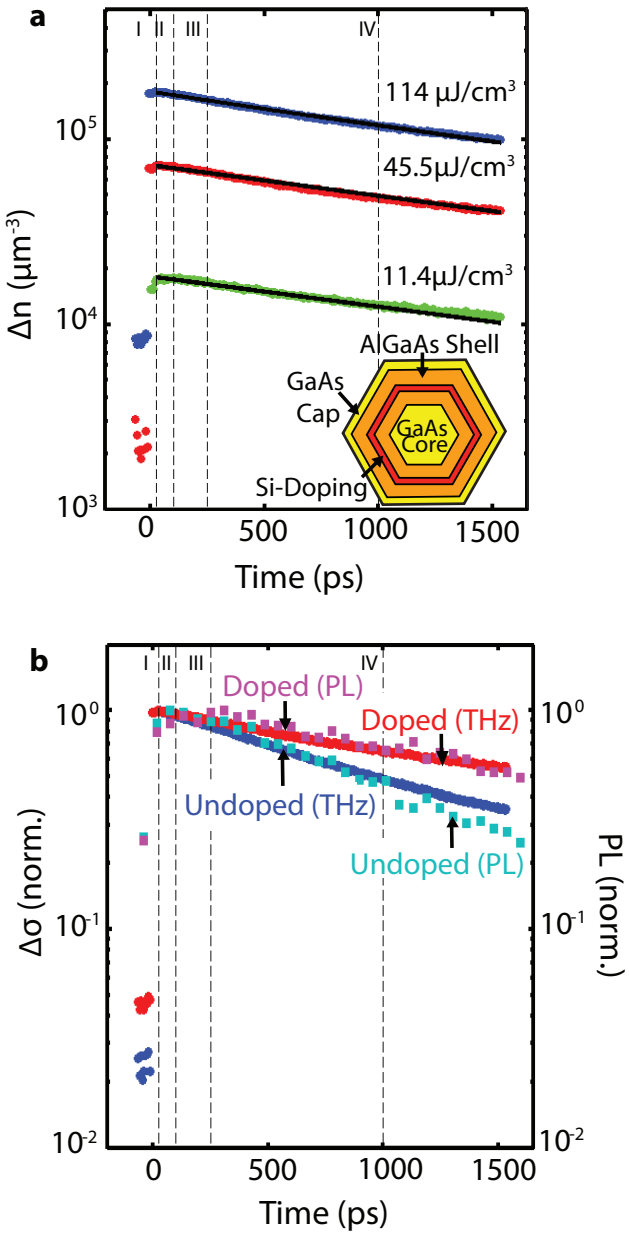

Figure 2: a) Photoinduced change of free electron concentration in modulation doped GaAs nanowires as a function of time after photoexcitation by 35 fs pulses of 1.55 eV photons at fluences of 11.4, 45.5, and 114 μJ cm^{-2} . I, II, III, IV represent delays of 25 ps, 100 ps, 250 ps and 1000 ps respectively. b) Comparison of the decay of normalised photoconductivity (circles) and normalised photoluminescence (squares) for modulation doped and undoped nanowires. The excitation fluence for the photoconductivity and PL experiments were 114 μJ cm^{-2} and 0.2 μJ cm^{-2} respectively, and PL was detected at a wavelength of 860 nm (corresponding to emission from the GaAs core). All measurements were performed at room temperature.

tion for the modulation doped sample at fluences of 11.4, 45.5, and 114 μJ cm^{-2}. The photoconductivity clearly shows a rapid rise within the first 5 ps after photoexcitation followed by a slow decay. The recombination dynamics of photoinjected electrons in a semiconductor may be described by the differential equation,[39]

$$\frac{dn\,(t)}{dt} = -k_1 n - k_2 n^2 - k_3 n^3, \tag{1}$$

where $n(t)$ is the electron density as a function of time, t, after photoexcitation. k_1 is a decay constant describing the rate of mono-molecular processes, such as trap-assisted recombination, recombination of photoinjected electrons with extrinsic holes or exciton recombination, the bimolecular recombination constant is given by k_2 and k_3 is the rate for Auger recombination.[40] In the OPTP experiments, the initial photoinjected electron density, $n(t = 0)$, may be freely set by adjusting the fluence of the laser pulse that photoexcites the sample. Thus by fitting Eqn. 1 to photoconductivity decay curves measured for a range of excitation fluences and setting k_1, k_2, and k_3 as global parameters, it is possible to determine these decay constants with a high degree of accuracy. Performing this global fitting procedure to the data shown in Figure 2a revealed decay constants for bimolecular and Auger recombination that were negligible ($k_2, k_3 \simeq 0$), leaving only a monomolecular term, $k_1 = 2.6 \pm 0.4 \times 10^8\,\mathrm{s}^{-1}$. Thus, the recombination is monoexponential with a photoinjected electron recombination lifetime of 3.9 ± 0.3 ns. The global fits are shown by the solid black lines in Figure 2a. As excitonic behaviour is not expected to dominate in this system at room temperature and the sample is n-type, the recombination mechanism for the modulation doped sample appears to be trap-assisted, as is typical for GaAs at room temperature.[29]

To better understand the mechanism of charge recombination, we also recorded the time resolved photoluminescence (PL) dynamics of single nanowires at room temperature and compared the results to the photoconductivity decays measured using the OPTP technique.

Single nanowires were excited with 100 fs laser pulses with a centre wavelength of 800 nm and a fluence of $0.2\,\mu J/cm^2$ and PL measured as a function of time after photoexcitation at a wavelength of 860 nm. The time resolved micro-PL setup is described in the Supporting Information.

Figure 2b shows a comparison between the room-temperature photoconductivity and PL lifetimes for both the modulation doped nanowires and the undoped reference. With OPTP, the signal measures the change in electron density as a function of time after photoexcitation, whereas the PL setup measures the rate of electron-hole recombination. Thus, the PL intensity is proportional to the product of the electron and hole density distributions and for PL to be seen, the electron and hole wavefunctions must spatially overlap.[41] It is clear from Figure 2b that for each sample the PL dynamics and photoconductivity dynamics are remarkably similar. This is in stark contrast to similar measurements on highly polytypic InP nanowires for which the PL emission decayed significantly faster than the photoconductivity due to spatial separation of the photoexcited electrons and holes.[41]

The photoconductivity lifetime for the modulation doped nanowires (3.9 ± 0.3 ns) is found to be significantly longer than for the undoped reference (1.5 ± 0.4 ns). Similarly, the PL lifetime of the modulation doped nanowire (2.39 ± 0.05 ns) is significantly longer than that of the undoped reference (1.1 ± 0.2 ns). The increase in the conductivity lifetime we observe as a result of modulation doping suggests that modulation doping passivates electron traps in the nanowires. As modulation doping is expected to generate high electron densities at the GaAs/$Al_{0.33}Ga_{0.67}As$ interfaces (see Figure 1b), it is thus likely that donated electrons passivate interfacial trap states located at the GaAs/$Al_{0.33}Ga_{0.67}As$ boundary.

In order to gain further insight into charge-carrier scattering and recombination mechanisms, photoconductivity spectra for both the modulation doped and undoped sample were measured. Figure 3 shows the photoconductivity spectra at an excitation fluence of $114\,\mu J\,cm^{-2}$ for both samples. Spectra were obtained at various delays of 25 ps, 100 ps, 250 ps and 1000 ps after photoexcitation. The conductivity spectra for both samples display a dis-

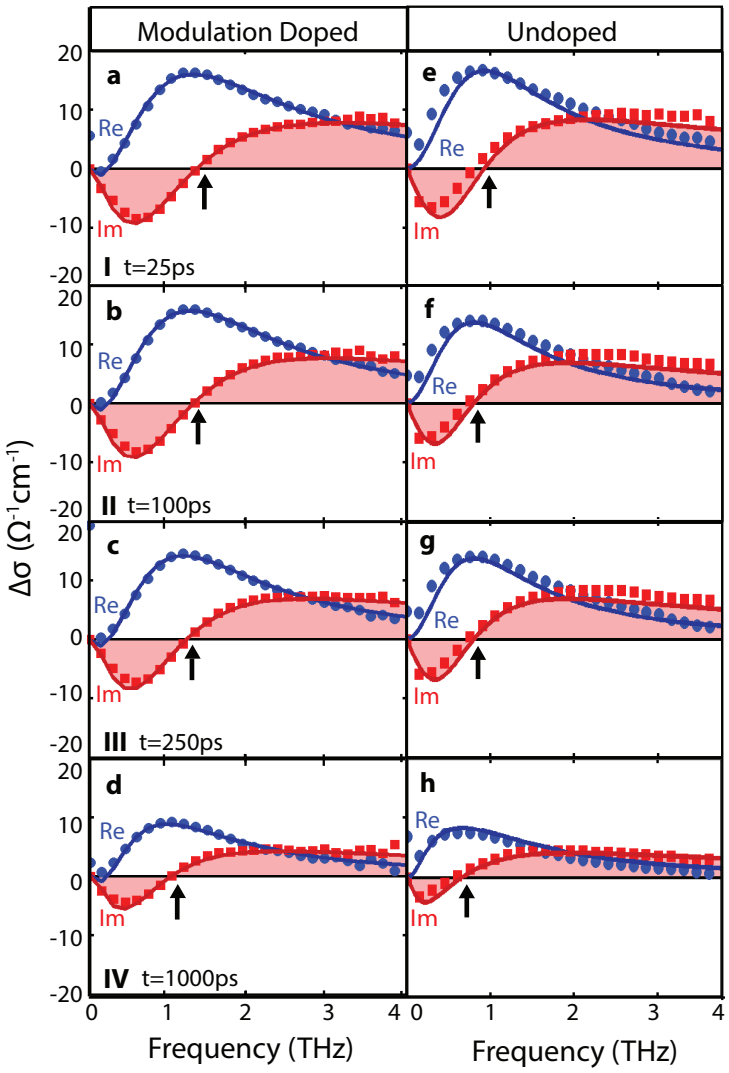

Figure 3: Time–resolved conductivity of photoexcited electrons for the n-type, modulation doped sample at times a) 25 ps, b) 100 ps, c) 250 ps and d) 1000 ps after photoexcitation; and for the undoped sample at times e) 25 ps f) 100 ps g) 250 ps and h) 1000 ps after photoexcitation. a)-d) correspond to times I, II, III, IV shown in Figure 2. The incident pump pulse excitation fluence was 114 μJ cm^{-2} for both samples. The symbols represent the measured data and the solid lines the fitted plasmon responses. The real (blue) and imaginary (red) components of the conductivity are plotted, with arrows indicating the resonant surface plasmon frequency, ω_0, for each spectrum. All measurements were performed at room temperature.

tinct Lorentzian response. The resonance clearly shifts to lower frequencies with time after photoexcitation, as can be seen from the arrows in Figure 3a-d and Figure 3e-h. The reduction of resonant frequency with decreasing electron density is a key attribute of localised surface plasmon (LSP) modes.[42] LSP modes have been well documented for metallic nanostructures, where the resonant frequency lies within the ultraviolet, visible and near infrared ranges.[43,44] For semiconductor nanostructures, which have a lower charge-carrier density than metallic nanostructures, the resonant frequency lies within the terahertz range.[29,45,46] We have previously shown that GaAs nanowires exhibit LSP modes within the terahertz range.[29,46,47]

The complex photoconductivity of a free electron plasma with a surface plasmon resonance is given by

$$\Delta\sigma = \frac{ine^2\omega}{m_e^*\left(\omega^2 - \omega_0^2 + i\omega\gamma\right)}, \tag{2}$$

where n is the electron density, e is the electronic charge, m_e^* is the effective electron mass, and γ is the momentum scattering rate. ω_0 is the surface plasmon resonant frequency given by

$$\omega_0(n) = \sqrt{\frac{fne^2}{m_e^*\epsilon_r\epsilon_0}}, \tag{3}$$

where ϵ_r is the dielectric constant of GaAs nanowires at terahertz frequencies, ϵ_0 is the permittivity of free space, and f is a constant that depends on the nanowire geometry and surrounding dielectric medium.[47] For doped samples, there is a significant charge-carrier density present without photoexcitation and the complex photoconductivity expression must therefore be modified.[41] When both intrinsic and extrinsic electrons are considered, with an equilibrium electron density before photoexcitation of n_d, the complex photoconductivity

then becomes:

$$\Delta\sigma = \frac{ie^2\omega}{m_e^*}\left[\frac{n_{\text{total}}}{\omega^2 - \{\omega_0(n_{\text{total}})\}^2 + i\omega\gamma} - \frac{n_d}{\omega^2 - \{\omega_0(n_d)\}^2 + i\omega\gamma}\right], \quad (4)$$

where $n_{\text{total}} = n_{\text{photo}} + n_d$ is the sum of the photoexcited and donated electon density.

The solid lines in Figure 3 show that Eqn. 4 provides an excellent fit to the measured photoconductivity spectra of both doped and undoped nanowire samples. For each sample, a global fitting routine was applied to all spectra at various times after photoexcitation, for which f was fixed at 0.25[41] and n_d was set as a global parameter, common to all spectra for the given sample. n_{photo} and γ were set to local fitting parameters for each spectrum, as the electron density and scattering rate vary with time after photoexcitation. For m_e^* and ϵ_r, the bulk values for GaAs of $0.063m_e^*$ and 12.95 were used respectively. From these fits, the doping level was then extracted. For the modulation doped sample, the donor density was found to be $1.10 \pm 0.06 \times 10^{16}\,\text{cm}^{-3}$, while for the undoped sample, it was found to be negligible within our measurement and fitting accuracy.

To confirm the validity of the model, photoconductivity spectra were also measured as a function of excitation fluence for both the modulation doped nanowires and the undoped reference. Spectra were recorded 100 ps after photoexcitation by 1.55 eV ($\lambda = 800$ nm) photons of eight different excitation fluences between $6.46\,\mu\text{J}\,\text{cm}^{-2}$ and $225\,\mu\text{J}\,\text{cm}^{-2}$ (the spectra are shown in Figure S6 of the Supporting Information). The results of globally fitting these spectra with Eqn. 4 are summarised in Figure 4a, which shows the extracted plasmon frequency, $\omega_0\,(n_{\text{total}})$, plotted against the square-root of the photoinjected electron density, $\sqrt{n_{\text{photo}}}$. For the undoped sample (blue line), as expected, a linear relationship is seen $\omega_o \propto \sqrt{n_{\text{photo}}}$, however for the doped sample (red line) a deviation from the linear relationship occurs. This deviation comes from the non-zero electron concentration, n_d, prior to photoexcitation. The value for the donated electron concentration from the global fit of the fluence dependent data was $n_d = 1.07 \pm 0.12 \times 10^{16}\,\text{cm}^{-3}$, which showed excellent

agreement with the independently measured value of $1.10 \pm 0.06 \times 10^{16}\,\mathrm{cm}^{-3}$ determined from photoconductivity spectra measured as a function of time after photoexcitation.

The mobility of electrons from both the modulation doped and undoped nanowire samples are shown in Figure 4b as a function of the total electron density, n_{total}. The mobility, μ, was calculated according to $\mu = \dfrac{e}{m_{\mathrm{e}}^{*}\gamma}$, using the scattering rates, γ, extracted from the previously described global fits to the photoconductivity spectra displayed in Figure 3. As can be seen from Figure 4b, the mobility was electron density dependent and ranged from $1680 \pm 100\,\mathrm{cm}^2\mathrm{V}^{-1}\mathrm{s}^{-1}$ to $2200 \pm 300\,\mathrm{cm}^2\mathrm{V}^{-1}\mathrm{s}^{-1}$ for the modulation doped sample; and between $2300 \pm 120\,\mathrm{cm}^2\mathrm{V}^{-1}\mathrm{s}^{-1}$ and $2960 \pm 290\,\mathrm{cm}^2\mathrm{V}^{-1}\mathrm{s}^{-1}$ for the undoped sample.

Importantly, no significant degradation of mobility is observed for the modulation doped sample compared with the undoped reference sample for similar values of electron density. In previous doping studies, impurity scattering has been found to reduce the electron mobility in doped GaAs nanowires,[15] while from our results it is clear that modulation doping does not degrade mobility. Figure 4b shows that at a total electron density value of approximately $3.5 \times 10^{16}\,\mathrm{cm}^{-3}$, the electron mobility for both samples is similarly high at approximately $2200\,\mathrm{cm}^2\mathrm{V}^{-1}\mathrm{s}^{-1}$, regardless of carriers being injected through doping or photoexcitation. Furthermore, the electron mobility for both samples decrease with increasing electron density, due to an increase in carrier–carrier scattering.

An empirical, low-field mobility model for III-V compounds was used to fit the mobility data. The model has been described previously[48] and is presented in the Supporting Information. It states that the extracted mobilities when plotted against n_{total} should take the following form:

$$\mu = \mu_{\mathrm{min}} + \frac{\mu_{\mathrm{max}} - \mu_{\mathrm{min}}}{1 + \left(\dfrac{n_{\mathrm{ref}}}{n}\right)^{\lambda}}, \tag{5}$$

where μ_{min} is the minimum electron mobility and μ_{max} the maximum electron mobility for the system, n_{ref} is the electron concentration at which the mobility reduces to half its

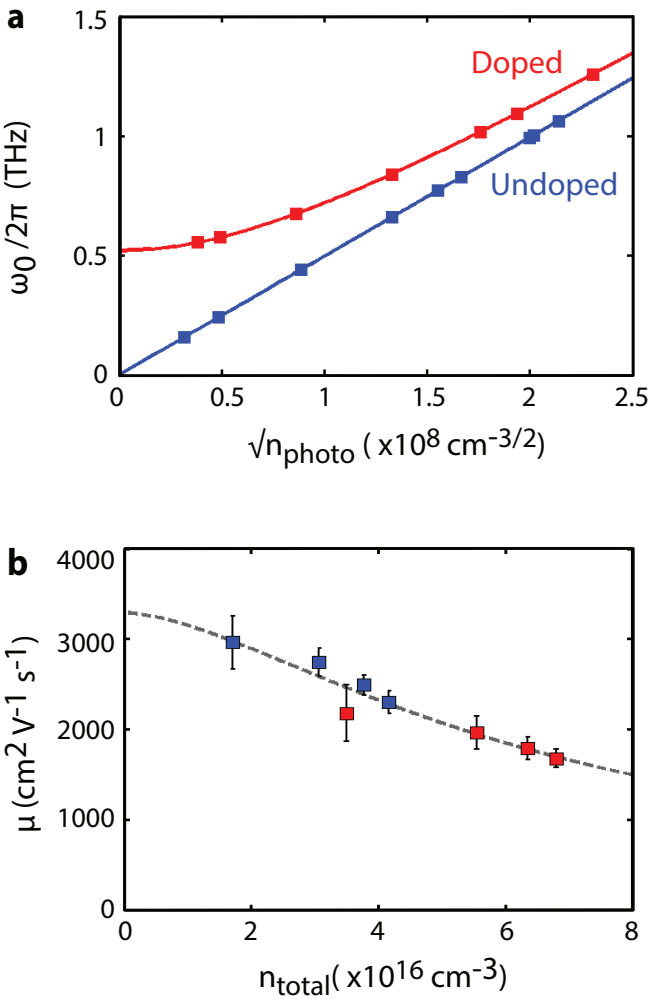

Figure 4: a) Plasmon frequency, $\omega_0\,(n_{\text{total}})$, plotted against the square-root of the photoexcited electron density, $\sqrt{n_{\text{photo}}}$, for the modulation doped (red squares) and undoped (blue squares) nanowire samples. Each data point corresponds to a fit of $\omega_0(n_{\text{total}})$ (via Eqn. 4) to a conductivity spectrum of nanowires photoexcited at a set fluence. These 16 fluence dependent conductivity spectra are shown in Figure S6 of the Supporting Information. The solid red line shows Eqn. 3 with $f = 0.25$, $n = n_{\text{total}}$ and doping density of $n_{\text{d}} = 1.07 \pm 0.12 \times 10^{16}\,\text{cm}^{-3}$ for the modulation doped sample. The corresponding curve with $n_{\text{d}} = 0$ is shown in blue. b) Room temperature electron mobility extracted for the modulation doped (red squares) and undoped sample (blue squares) plotted against the total electron density n_{total}. These data were extracted from the fits displayed in Figure 3. The dashed line represents a fit to Eqn. 5 which is an empirical, low-field model of electron mobility.

maximum value at low doping and λ is a scaling factor related to the material. At high doping concentrations, the mobility saturates at $\mu_{\min}$, which is temperature-independent; and at very low doping concentrations, the mobility saturates at $\mu_{\max}$, which is the lattice-limited mobility and reduces with increasing temperature. By fitting this equation to all the extracted mobility points with fitted values of $\lambda = 1.63$ and $n_{\mathrm{ref}} = 6.34 \pm 0.25 \times 10^{17}\,\mathrm{cm}^{-3}$, a minimum electron mobility of $680 \pm 120\,\mathrm{cm}^2\mathrm{V}^{-1}\mathrm{s}^{-1}$ and a maximum electron mobility of $3290 \pm 20\,\mathrm{cm}^2\mathrm{V}^{-1}\mathrm{s}^{-1}$ were obtained. As the model, which only takes into account carrier–carrier scattering, fits the measured mobilities for both the modulation doped and undoped samples, it can be deduced that modulation doping avoids the reduction in electron mobility associated with bulk doping. As the total electron concentration increases with n-type modulation doping, a reduction in mobility occurs as a result of carrier-carrier scattering. However, when the increased electron density of the modulation doped sample is considered only a small reduction in electron mobility is observed, as can be seen in Figure 4 where the extracted mobilities coincide with the empirical model. This minimal reduction in electron mobility is due to the dopants being situated away from the interface, reducing scattering of charge-carriers in the core of the nanowire with ionised dopants. Thus, modulation doped GaAs nanowires provide a high electron mobility of $2200 \pm 300\,\mathrm{cm}^2\mathrm{V}^{-1}\mathrm{s}^{-1}$ suggesting that n-type modulation doping could be highly attractive for nanowire applications in future optoelectronic devices.

However there is still much to be done to further improve the electron mobility in semiconductor nanowires. Even considering the effect of carrier–carrier scattering, the upper electron mobility values $\mu_{\max}$ for both the modulation doped and undoped reference nanowire samples are significantly lower than those for bulk GaAs.[49] Electron scattering at the nanowire surfaces is likely to be a significant contributing factor for nanowires owing to the large surface area-to-volume ratio of nanowires. Thus optimised surface passivation[50] is an important route to increasing the electron mobility in nanowires. Furthermore, polytypism, which was significant in our samples (see Figures S1 and S2 of the Supporting Information), is also

likely to be a contributing factor to this reduction in mobility from bulk values and could be minimised with pure-phase structures, as we have shown previously.[30] In addition it was recently shown that electron mobility can also be enhanced by increasing the nanowire shell thickness.[51]

In conclusion, we have presented the first non-contact terahertz frequency measurements of the electronic properties of modulation doped GaAs nanowires. Terahertz spectroscopy, in particular the OPTP spectroscopy technique, provides an ideal tool for accurately measuring the photoconductivity lifetime, electron mobility and also the doping levels in nanowires. We have demonstrated that core–shell, GaAs nanowires can be successfully grown with an extrinsic electron concentration of $1.10 \pm 0.06 \times 10^{16}\,\mathrm{cm}^{-3}$. The photoconductivity and photoluminescence lifetimes were found to be $3.92 \pm 0.27\,\mathrm{ns}$ and $2.39 \pm 0.05\,\mathrm{ns}$ at room tempertaure. These lifetimes are considerably longer than has been seen for GaAs or other III-V nanowires previously, highlighting the potential of these modulation doped nanostructures for future optoelectronic and photovoltaic devices. A value for the room-temperature electron mobility was also extracted from the photoconductivity spectra and found to be $2200 \pm 300\,\mathrm{cm}^2\mathrm{V}^{-1}\mathrm{s}^{-1}$. This value is high for GaAs nanowires and shows that there is no significant degradation of the electron mobility when compared to an undoped reference. Therefore, modulation doping appears to be an excellent way of controlling conductivity in semiconductor nanowires while retaining a high electron mobility, and OPTP spectroscopy offers a rapid non-contact method of characterising and hence further improving the electrical properties of these heterostructures.

Acknowledgement

The authors thank the EPSRC (U.K.) for financial support. The Swiss National Science Foundation via projects nr137648 and 156081 and the NCCR-QSIT is greatly acknowledged. H.J.J thanks the Royal Commission for the Exhibition of 1851 for her research fellowship.

Supporting Information Available

Description of experiments (nanowire growth, sample preparation, electron microscopy, terahertz time-domain spectroscopy, time-resolved micro-photoluminescence); TEM images of doped and undoped sample; Schrödinger-Poisson simulation results for photoexcited nanowires; photoconductivity dynamics data for undoped nanowires as a function photoexcitation-fluence; photoconductivity spectra as a function of photoexcitation-fluence for both doped and undoped nanowires; details of data analysis (calculations for converting terahertz transmission data to photoconductivity, descriptions of rate equations used for modelling of time resolved conductivity data, description of empirical model used for fitting mobilities from photoconductivity spectra) can all be found in the Supporting Information.

This material is available free of charge via the Internet at `http://pubs.acs.org/`.

References

(1) Li, Y.; Qian, F.; Xiang, J.; Lieber, C. M. *Mater. Today* **2006**, *9*, 18.

(2) Czaban, J. A.; Thompson, D. A.; Lapierre, R. R. *Nano Lett.* **2009**, *9*, 148–154.

(3) Tian, B.; Kempa, T. J.; Lieber, C. M. *Chem. Soc. Rev.* **2009**, *38*, 16–24.

(4) Law, M.; Greene, L. E.; Johnson, J. C.; Saykally, R.; Yang, P. D. **2005**, *4*, 455–459.

(5) Gradevcak,; Qian, F.; Li, Y.; Park, H.; Lieber, C. M. *Appl. Phys. Lett.* **2005**, *87*, 173111.

(6) Duan, X. F.; Huang, Y.; Agarwal, R.; Lieber, C. M. *Nature* **2003**, *421*, 241.

(7) Duan, X. F.; Huang, Y.; Cui, Y.; Wang, J. F.; Lieber, C. M. *Nature* **2001**, *409*, 66–69.

(8) Minot, E. D.; Kelkensberg, F.; Kouwenhoven, L. P.; Zwiller, V.; Borgström, M. T.; Wunnicke, O.; Verheijen, M. A.; Bakkers, E. P. A. M. *Nano Lett.* **2007**, *7*, 367–371.

(9) Haraguchi, K.; Katsuyama, T.; Hiruma, K.; Ogawa, K. *Appl. Phys. Lett.* **1992**, *60*, 745–747.

(10) Dimakis, E.; Ramsteiner, M.; Tahraoui, A.; Riechert, H.; Geelhaar, L. *Nano Res.* **2012**, *5*, 796–804.

(11) Gutsche, C.; Lysov, A.; Regolin, I.; Blekker, K.; Prost, W.; Tegude, F. J. *Nanoscale Res. Lett.* **2011**, *6*, 65.

(12) Gutsche, C.; Regolin, I.; Blekker, K.; Lysov, A.; Prost, W.; Tegude, F. J. *J. Appl. Phys.* **2009**, *105*, 024305.

(13) Salehzadeh, O.; Zhang, X.; Gates, B. D.; Kavanagh, K. L.; Watkins, S. P. *J. Appl. Phys.* **2012**, *112*, 094323.

(14) Zhang, P.; Liu, Y.; Guo, J. W.; Zhang, X. P. **2013**, *774*, 860–863.

(15) Ketterer, B.; Uccelli, E.; i Morral, A. F. *Nanoscale* **2012**, *4*, 1789–1793.

(16) Ponseca, C. S.; Němec, H.; Wallentin, J.; Anttu, N.; Beech, J. P.; Iqbal, A.; M, B.; Pistol, M. E.; Samuelson, L.; Yartsev, A. *Phys. Rev. B* **2014**, *90*, 085405.

(17) Pfeiffer, L.; West, K. W.; Stormer, H. L.; Baldwin, K. W. *Appl. Phys. Lett.* **1989**, *55*, 1888–1890.

(18) Zervos, M. *Phys. Status Solidi-Rapid Res. Lett.* **2013**, *7*, 651–654.

(19) Wallentin, J.; Borgström, M. T. *J. Mater. Res.* **2011**, *26*, 2142–2156.

(20) Hilse, M.; Ramsteiner, M.; Breuer, S.; Geelhaar, L.; Riechert, H. *Appl. Phys. Lett.* **2010**, *96*, 193104.

(21) Casadei, A.; Krogstrup, P.; Heiss, M.; Rohr, J. A.; Colombo, C.; Ruelle, T.; Upadhyay, S.; Sorensen, C. B.; Nygard, J.; Morral, A. F. I. *Appl. Phys. Lett.* **2013**, *102*, 013117.

(22) Dufouleur, J.; Colombo, C.; Garma, T.; Ketterer, B.; Uccelli, E.; Nicotra, M.; Morral, A. F. I. *Nano Lett.* **2010**, *10*, 1734–1740.

(23) Ketterer, B.; Mikheev, E.; Uccelli, E.; Morral, A. F. I. *Appl. Phys. Lett.* **2010**, *97*, 223103.

(24) Jadczak, J.; Plochocka, P.; Mitioglu, A.; Breslavetz, I.; Royo, M.; Bertoni, A.; Goldoni, G.; Smolenski, T.; Kossacki, P.; Kretinin, A.; Shtrikman, H.; Maude, D. K. *Nano Lett.* **2014**, *14*, 2807–2814.

(25) Sladek, K.; Klinger, V.; Wensorra, J.; Akabori, M.; Hardtdegen, H.; Grutzmacher, D. *J. Cryst. Growth* **2010**, *312*, 635–640.

(26) Spirkoska, D.; i Morral, A. F.; Dufouleur, J.; Xie, Q.; Abstreiter, G. *Phys. Status Solidi-Rapid Res. Lett.* **2011**, *5*, 353–355.

(27) Cui, Z. X.; Perumal, R.; Ishikura, T.; Konishi, K.; Yoh, K.; Motohisa, J. *Appl. Phys. Express* **2014**, *7*, 085001.

(28) Joyce, H. J.; Gao, Q.; Tan, H. H.; Jagadish, C.; Kim, Y.; Zou, J.; Smith, L. M.; Jackson, H. E.; Yarrison-Rice, J. M.; Parkinson, P.; Johnston, M. B. *Prog. Quantum Electron.* **2011**, *35*, 23–75.

(29) Joyce, H. J.; Docherty, C. J.; Gao, Q.; Tan, H. H.; Jagadish, C.; Lloyd-Hughes, J.; Herz, L. M.; Johnston, M. B. *Nanotechnology* **2013**, *24*, 214006.

(30) Parkinson, P.; Joyce, H. J.; Gao, Q.; Tan, H. H.; Zhang, X.; Zou, J.; Jagadish, C.; Herz, L. M.; Johnston, M. B. *Nano Lett.* **2009**, *9*, 3349–3353.

(31) Yong, C. K.; Noori, K.; Gao, Q.; Joyce, H. J.; Tan, H. H.; Jagadish, C.; Giustino, F.; Johnston, M. B.; Herz, L. M. *Nano Lett.* **2012**, *12*, 6293–6301.

(32) Thunich, S.; Prechtel, L.; Spirkoska, D.; Abstreiter, G.; Morral, A. F. I.; Holleitner, A. W. *Appl. Phys. Lett.* **2009**, *95*, 083111.

(33) Lucot, D.; Jabeen, F.; Ramdani, M. R.; Patriarche, G.; Faini, G.; Mailly, D.; Harmand, J. C. *J. Cryst. Growth* **2013**, *378*, 546–548.

(34) Storm, K.; Halvardsson, F.; Heurlin, M.; Lindgren, D.; Gustafsson, A.; Wu, P. M.; Monemar, B.; Samuelson, L. *Nat. Nanotechnol.* **2012**, *7*, 718–722.

(35) Funk, S. et al. *Nano Lett.* **2013**, *13*, 6189–6196.

(36) Maharjan, A.; Pemasiri, K.; Kumar, P.; Wade, A.; Smith, L. M.; Jackson, H. E.; Yarrison-rice, J. M.; Kogan, A.; Paiman, S.; Gao, Q.; Tan, H. H.; Jagadish, C. *Appl. Phys. Lett.* **2009**, *94*, 193115.

(37) Birner, S.; Zibold, T.; Andlauer, T.; Kubis, T.; Sabathil, M.; Trellakis, A.; Vogl, P. *IEEE Trans. Electron Devices* **2007**, *54*, 2137–2142.

(38) Lloyd-Hughes, J.; Jeon, T.-I. *J Infrared Milli Terahz Waves* **2012**, *33*, 871.

(39) Aspnes, D. E. *Surf. Sci.* **1983**, *132*, 406–421.

(40) Wehrenfennig, C.; Eperon, G. E.; Johnston, M. B.; Snaith, H. J.; Herz, L. M. *Adv. Mater.* **2014**, *26*, 1584–1589.

(41) Joyce, H. J.; Wong-Leung, J.; Yong, C.; Docherty, C. J.; Paiman, S.; Gao, Q.; Tan, H. H.; Jagadish, C.; Lloyd-Hughes, J.; Herz, L. M.; Johnston, M. B. *Nano Lett.* **2012**, *12*, 5325–5330.

(42) Nienhuys, H.-K.; Sundström, V. *Appl. Phys. Lett.* **2005**, *87*, 012101.

(43) Barnes, W. L.; Dereux, A.; Ebbesen, T. W. *Nature* **2003**, *424*, 824–830.

(44) Barnes, W. L. *J. Opt. A-Pure Appl. Opt.* **2006**, *8*, S87.

(45) Isaac, T. H.; Barnes, W. L.; Hendry, E. *Appl. Phys. Lett.* **2008**, *93*, 241115.

(46) Kužel, P.; Němec, H. *J. Phys. D-Appl. Phys.* **2014**, *47*, 374005.

(47) Parkinson, P.; Lloyd-Hughes, J.; Gao, Q.; Tan, H. H.; Jagadish, C.; Johnston, M. B.; Herz, L. M. *Nano Lett.* **2007**, *7*, 2162–2165.

(48) Sotoodeh, M.; Khalid, A. H.; Rezazadeh, A. A. *J. Appl. Phys.* **2000**, *87*, 2890–2900.

(49) Beard, M. C.; Turner, G. M.; Schmuttenmaer, C. A. *Phys. Rev. B* **2000**, *62*, 15764–15777.

(50) Chang, C.; Chi, C.; Yao, M.; Huang, N.; Chen, C.; Theiss, J.; Bushmaker, A. W.; LaLumondiere, S.; Yeh, T.; Povinelli, M. L.; Zhou, C.; Dapkus, P. D.; Cronin, S. B. *Nano Lett.* **2012**, *12*, 4484–4489.

(51) Joyce, H. J.; Parkinson, P.; Jiang, N.; Docherty, C. J.; Gao, Q.; Tan, H. H.; Jagadish, C.; Herz, L. M.; Johnston, M. B. *Nano Lett.* **2014**, *14*, 5989–5994.

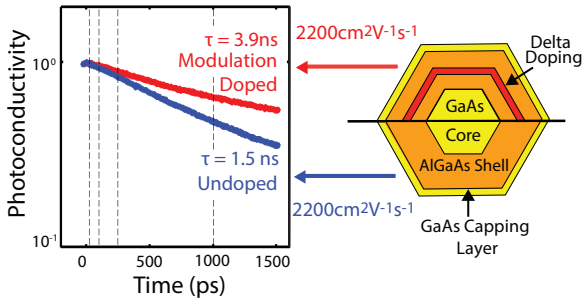

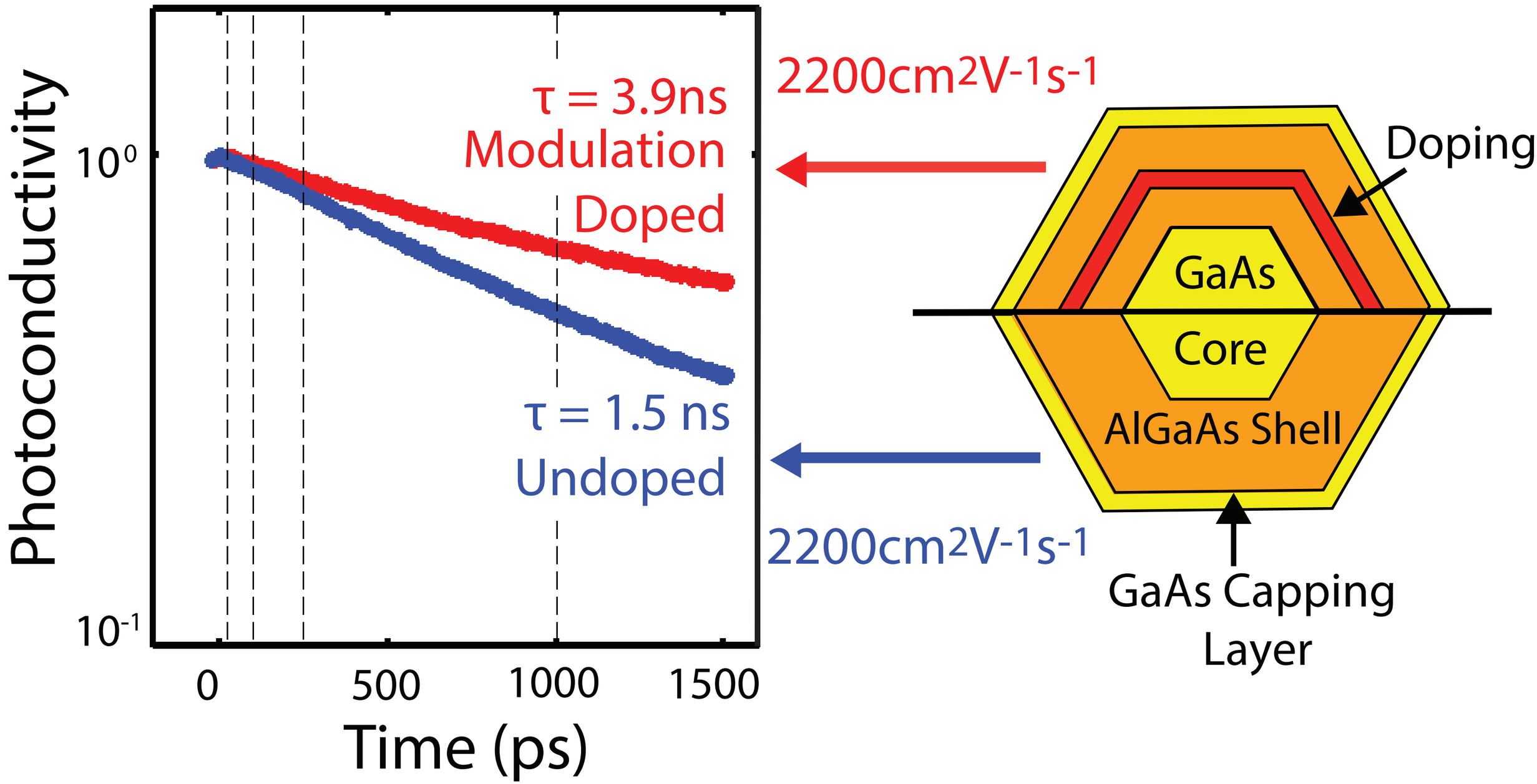
Photoconductivity
10^0
10^{-1}
0
500
1000
1500
Time (ps)
τ = 3.9ns
Modulation
Doped
τ = 1.5 ns
Undoped
2200cm²V⁻¹s⁻¹
2200cm²V⁻¹s⁻¹
Doping
GaAs
Core
AlGaAs Shell
GaAs Capping
Layer